A supramolecular chemistry approach for potentiating live attenuated whole-organism vaccines

Duszenko, N.

2

A supramolecular platform technology for bacterial cell surface modification

Nikolas Duszenko, Danny M. van Willigen, Mick M. Welling, Clarize M. de Korne, Roos van Schuijlenburg, Beatrice M.F. Winkel, Fijs W.B. van Leeuwen and Meta Roestenberg

Adapted from:

ACS Infect Dis. 2020 Jul 10;6(7): 1734-1744.
PMID: 32364374
DOI: 10.1021/acsinfecdis.9b00523.

Abstract

In an era of antimicrobial resistance, a better understanding of the interaction between bacteria and the sentinel immune system is needed to discover new therapeutic targets for combating bacterial infectious disease. Sentinel immune cells such as macrophages phagocytose intact bacteria and thereby initiate ensuing immune responses. Bacterial surface composition is a key element which determines macrophage signaling. To study the role of bacterial cell surface composition in immune recognition, we developed a platform technology for altering bacterial surfaces in a controlled manner with versatile chemical scaffolds. We show that these scaffolds are efficiently loaded onto both Gram-positive and -negative bacteria, and that their presence does not impair the capacity of monocyte-derived macrophages to phagocytose bacteria and subsequently signal to other components of the immune system. We believe this technology thus presents a useful tool to study the role of bacterial cell surface composition in disease etiology and potentially for novel interventions utilizing intact bacteria for vaccination.

Introduction

The rise of drug-resistant bacteria has led to the reemergence of bacterial infectious diseases once thought vanquished with the discovery of antibiotics (Willyard, 2017). Novel vaccines and drugs are needed to combat this growing threat. A better understanding of the interactions between bacteria and the immune system can facilitate the identification of new targets for interventions.

Interactions between bacteria and the immune system are initiated by cells of the innate immune system, such as macrophages (MΦs). These cells are responsible for orchestrating the ensuing immune response (Wynn et al., 2013). MΦs are able to recognize bacteria by their size and unique bacterial cell wall components (Kumar et al., 2011; Mogensen, 2009). These features prompt the MΦ to internalize the bacteria by phagocytosis and degrade them. Doing so liberates the bacterial cell wall components, which dose-dependently trigger intracellular signaling cascades that modulate MΦ effector functions (Wolf and Underhill, 2018). The bacterial cell wall composition is thus thought to be responsible for the large heterogeneity in bacteria-host interactions, ranging from the vigorous systemic inflammatory response syndromes seen with Gram-negative bacteria such *Escherichia coli* to the comparatively weak responses to many Gram-positive bacteria like *Staphylococcus aureus* (Annane et al., 2005; Goldmann and Medina, 2018).

A single bacterial cell surface component of Gram-negative bacteria, lipopolysaccharide (LPS), is responsible for the previously mentioned systemic inflammatory response syndromes. LPS potency in priming immune responses has been utilized in vaccine development, where chemically modified LPS variants have been successfully used to create potent new vaccines for hepatitis B and human papillomavirus (Kong et al., 2008; Paavonen et al., 2009). Bacteria like the Gram-positive *S. aureus* lack highly immunogenic components such as LPS, resulting in dampened immune responses which allow *S. aureus* to establish chronic infections that the immune system is unable to clear (Bekeredjian-Ding et al., 2017; Naber, 2009). Other pathogenic bacteria have instead evolved modifications of immunogenic components that render them inert. There are for example a number of Gram-negative bacterial species, like *Salmonella enterica* and *Helicobacter pylori*, whose unusual LPS structure does not elicit a proper immune response (Maldonado et al., 2016). Much like *S. aureus*, these bacteria can establish chronic infections. Further unraveling which bacterial cell wall components are responsible for directing MΦ responses is thus an important step in advancing our understanding of interactions between bacteria and the immune system.

To study the role of bacterial cell wall components in early immune responses, we envisioned a tool which would allow us to alter the bacterial cell wall in a

controlled manner without disturbing the bacteria's structural integrity. Reproducible chemical modification of (bacterial) cell surfaces is in itself a challenging endeavor, but doing so in the context of introducing immunomodulatory compounds presents unique challenges (Bi et al., 2018; Gautam et al., 2013; Mongis et al., 2017). As immune responses are influenced by immunomodulator quantity, it is essential to clearly define loading rates. One way of doing this is by using a generic chemical platform that standardizes the loading rate regardless of the compound being introduced. Recently, we have developed pre-targeting methods which enable precise quantification of loading rate. By harnessing supramolecular chemistry we reproducibly loaded macro-aggregated albumin (MAA) microparticles and eukaryotic cells with scaffolds that remained stable under chemically challenging *in vitro* and *in vivo* conditions (Rood et al., 2017; Spa et al., 2018; Welling et al., 2019). The multivalent host-guest interactions between β-cyclodextrin (CD) and adamantane (Ad) underpinning these scaffolds have already found widespread use for controllably introducing various chemical and biological functionalities onto inorganic svurface (Gonzalez-Campo et al., 2010; Neirynck et al., 2013; Rodell et al., 2015). We thus reasoned that these scaffolds might similarly be used as a generic chemical platform for controllably introducing (immunomodulatory) components onto bacterial cells while preserving viability and original biological composition.

The aim of this study was to investigate the use of supramolecular scaffolds as a generic chemical platform to modify bacterial cell surface composition. To this end, we first assessed the loading of our supramolecular scaffolds onto both Gram-positive (*Staphylococcus aureus*) and Gram-negative (*Escherichia coli*) bacteria, using MAA microspheres as a validated control. We then assayed the effects of these scaffolds on MΦ responses.

Results

In this study we used three different entities to investigate the loading of a chemical scaffold **Cy3$_{1.5}$CD$_{100}$PIBMA$_{389}$** onto bacterial cell surfaces and the resultant effects on MΦ recognition and response as gauged by three major immunological parameters – phagocytosis, surface marker expression and cytokine production – using a monocyte-derived MΦ (MoMΦ) assay (Figure 1).

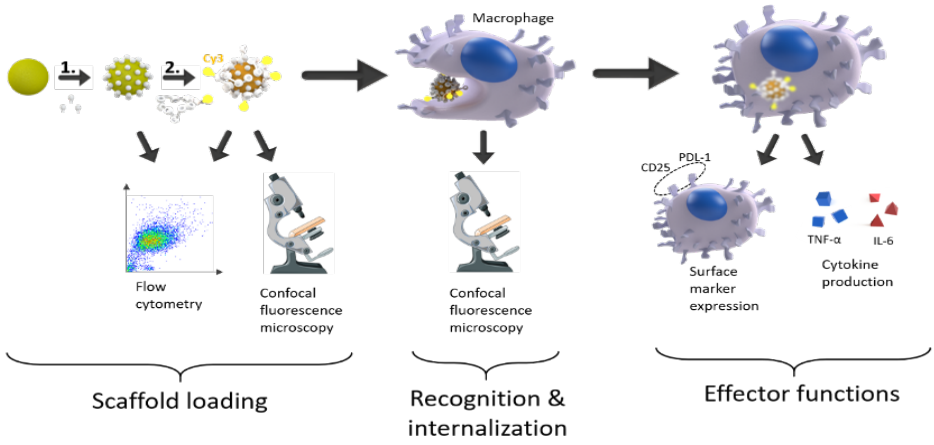

Figure 1: Experimental setup of the described study. Schematic illustrating the process by which the scaffold **Cy3$_{1.5}$CD$_{100}$PIBMA$_{389}$** was loaded onto three different entities and its concomitant effects on immune responses were assessed. The surface of each entity was first functionalized with adamantane (**1.**), followed by **Cy3$_{1.5}$CD$_{100}$PIBMA$_{389}$** loading (**2.**). The presence of loaded scaffold was then confirmed by flow cytometry and confocal fluorescence microscopy. Thereafter, the ability of MoMΦ to recognize and internalize **Cy3$_{1.5}$CD$_{100}$PIBMA$_{389}$**-loaded entities was analyzed by confocal fluorescence microscopy. Finally, MoMΦ effector functions in response to **Cy3$_{1.5}$CD$_{100}$PIBMA$_{389}$**-loaded entities – as gauged by surface marker expression and cytokine

Cy3$_{1.5}$CD$_{100}$PIBMA$_{389}$ is a versatile scaffold that is efficiently loaded onto both Gram-positive and -negative bacteria

Our experimental setup was first validated using 10-20 μm MAA microspheres. To assess whether functionalizing MAA by conjugating Ad to the primary amines of lysine residues via amide linkages was a promising strategy, we used an analogous reagent to couple Cy5 to MAA via amide linkages. Flow cytometric analysis of the resulting Cy5 signal showed this to be an efficient process (Figure 2ai, 2aii). We next confirmed the loading of **Cy3$_{1.5}$CD$_{100}$PIBMA$_{389}$** onto Ad-functionalized MAA by confocal fluorescence microscopy (Figure 3a). Flow cyto-

metric analysis showed **Cy3$_{1.5}$CD$_{100}$PIBMA$_{389}$** loading (Figure 4ai) to be highly efficient, resulting in 98.5±0.25% MAA particles loaded with **Cy3$_{1.5}$CD$_{100}$PIBMA$_{389}$**, and demonstrated that Ad functionalization facilitated **Cy3$_{1.5}$CD$_{100}$PIBMA$_{389}$** loading more than 2-fold (3,556±224 vs 1,606±668, $p < 0.01$, Figure 4aii).

We subsequently moved onto transferring our technology to *Staphylococcus aureus*, a Gram-positive bacterium, and *Escherichia coli*, a Gram-negative bacterium. Doing so involved an alternative Ad functionalization, where Ad was first conjugated to a cationic peptide (UBI$_{29-41}$) known to insert itself into bacterial cell membranes that served as a vector for then introducing Ad onto the bacterial cell surface (Welling et al., 2004). We assessed the feasibility of this approach using a Cy5-labeled UBI$_{29-41}$, and via flow cytometry observed UBI$_{29-41}$ to the efficiently incorporated into both *S. aureus* (Fig 2bi, 2bii) and *E. coli* (Figure 2ci, 2cii). Following this validation we confirmed loading of **Cy3$_{1.5}$CD$_{100}$PIBMA$_{389}$** via confocal fluorescence microscopy onto both Ad-functionalized *S. aureus* (Figure 3b) and *E. coli* (Figure 3c), as evinced by clear Cy3 surface signals that contrasted with Hoechst counterstaining of the cells' cytoplasm (Figure 3d, 3e). Subsequent flow cytometry analysis showed **Cy3$_{1.5}$CD$_{100}$PIBMA$_{389}$** loading rates of 99.5±0.1% for *S. aureus* (Figure 4bi) and 96.4±1.4% for *E. coli* (Figure 4ci). There was a discrepancy between our bacterial platforms regarding the importance of Ad functionalization for facilitating **Cy3$_{1.5}$CD$_{100}$PIBMA$_{389}$** loading: Ad$_2$-UBI$_{29-41}$ surface functionalization enhanced **Cy3$_{1.5}$CD$_{100}$PIBMA$_{389}$** loading to Gram-positive *S. aureus* more than 3-fold (51,786±1,999 vs 17,464±1,273, $p < 0.01$, Figure 4bii), whereas the increase was less than 2-fold for Gram-negative *E. coli* (64,519±10,083 vs 46,456±7,290, $p = 0.07$, Figure 4cii).

Previously, supramolecular host-guest chemistry on cell surfaces has been shown to not adversely affect cell viability (Rood et al., 2017). We similarly did not note any adverse effects of **Cy3$_{1.5}$CD$_{100}$PIBMA$_{389}$** loading on viability for *S. aureus* as gauged by colony counts (12.8±2.9 vs 12±3.3, $p = 0.66$, Figure 5a). However, *E. coli* viability did appear hampered by scaffold loading (4.5±1.5 vs 13.2±7.7, $p = 0.022$, Figure 5b).

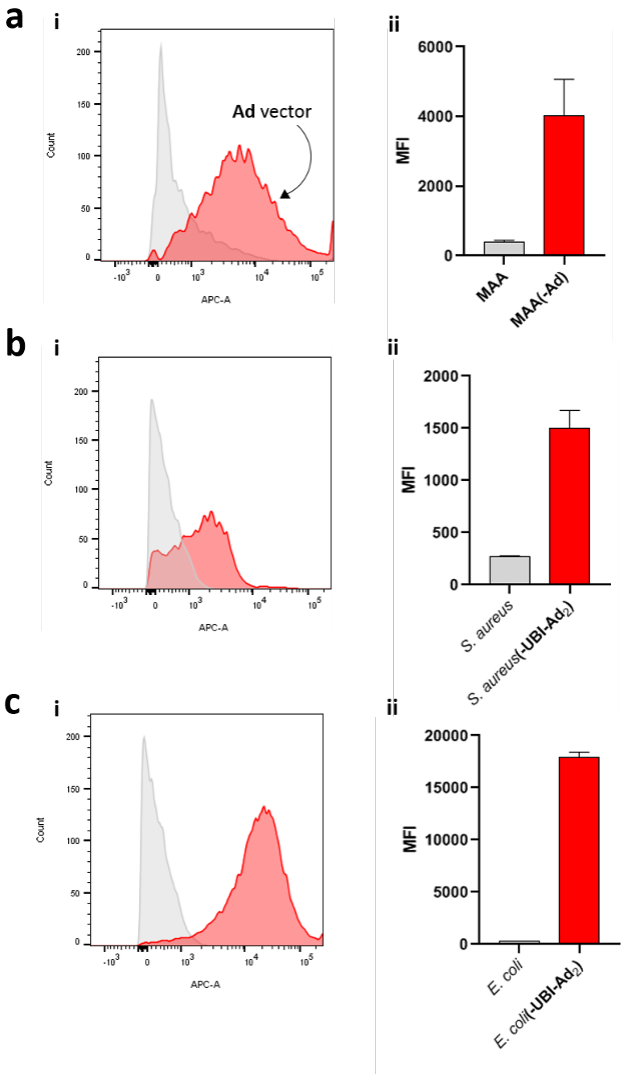

Figure 2: Ad functionalization efficiency for MAA (a), *S. aureus* (b) and *E. coli* (c). Potential Ad functionalization efficiency was assessed with the use of Cy5-labeled vectors (amide bond for MAA, UBI_{29-41} for bacteria) onto MAA/bacterial surfaces. After functionalization Cy5 signals were measured on a flow cytometer **(i)**. Median fluorescent intensities (MFI) of these Cy5 signals for functionalized MAA or bacteria (red) versus unlabeled controls (grey) are given in **(ii)** as means ± standard deviation for a representative experiment of n = 3. Ad = adamantane; MAA = macro-aggregated albumin.

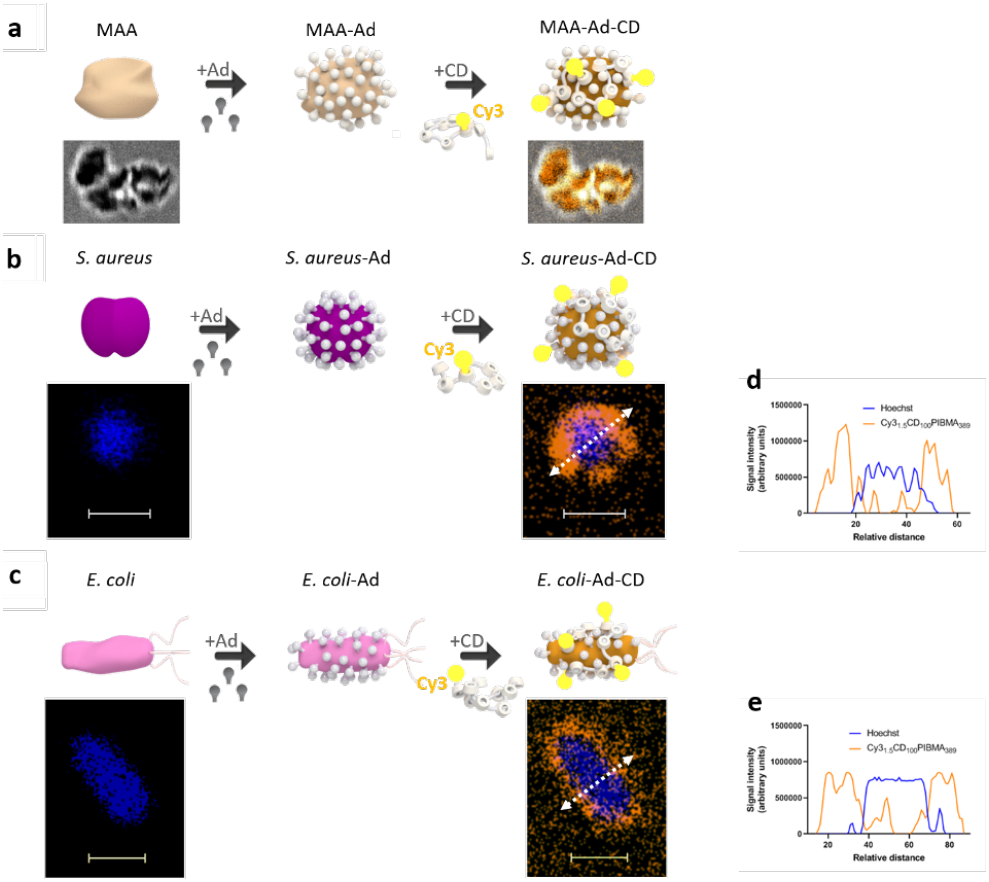

Figure 3: $Cy3_{1.5}CD_{100}PIBMA_{389}$ loading onto a microbial model (a) and two different bacteria (b)(c). Confocal fluorescence microscopy demonstrating the presence of **$Cy3_{1.5}CD_{100}PIBMA_{389}$** loaded onto MAA **(a)**; *S. aureus*, a typical Gram-positive bacterium **(b)**; and *E. coli*, a typical Gram-negative bacterium **(c)**. To assess the location of **$Cy3_{1.5}CD_{100}PIBMA_{389}$** on bacteria, the fluorescent signal intensities of Cy3 and Hoechst in a cross section of the bacteria were analyzed and plotted for *S. aureus* **(d)** and *E. coli* **(e)**. Scale bar = 1 µm. Ad = adamantane; CD = **$Cy3_{1.5}CD_{100}PIBMA_{389}$**; MAA = macro-aggregated albumin.

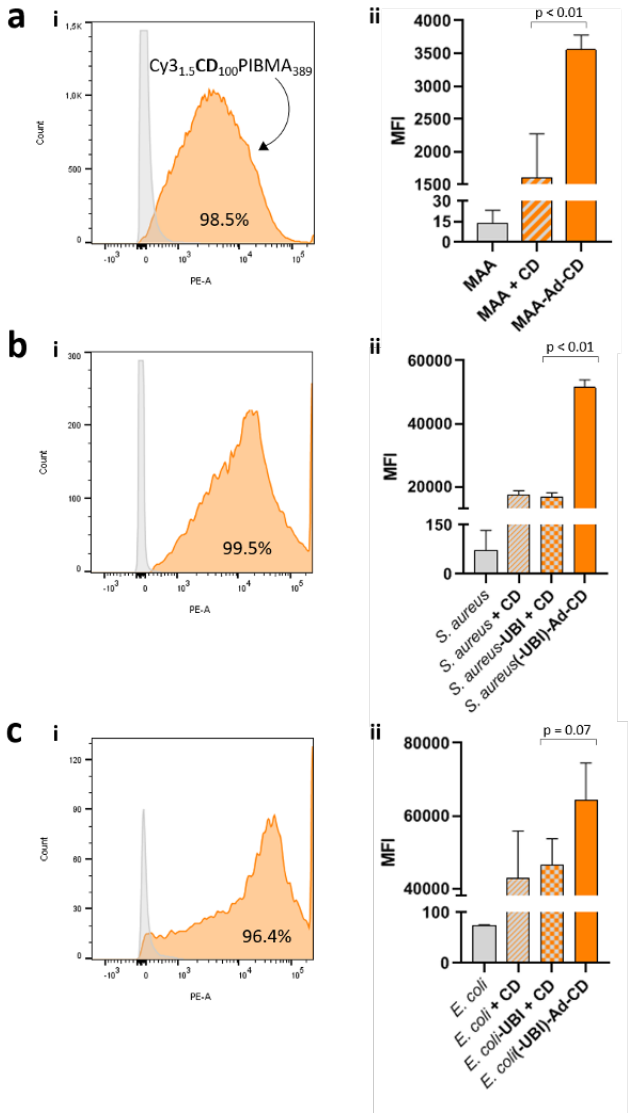

Figure 4: Cy3$_{1.5}$CD$_{100}$PIBMA$_{389}$ loading efficiency for MAA (a), *S. aureus* (b) and *E. coli* (c). Loading was assessed by measuring Cy3 signal intensities **(i)** on a flow cytometer. Median fluorescent intensities (MFI) of these Cy3 signals for loading in the presence of Ad (orange), loading without Ad but with UBI present (grey/orange checkers), loading without Ad and UBI (grey/orange stripes) and unloaded controls (grey) are given in **(ii)** as means ± standard deviation for a representative experiment of n = 3. CD = **Cy3$_{1.5}$CD$_{100}$PIBMA$_{389}$**; MAA = macro-aggregated albumin.

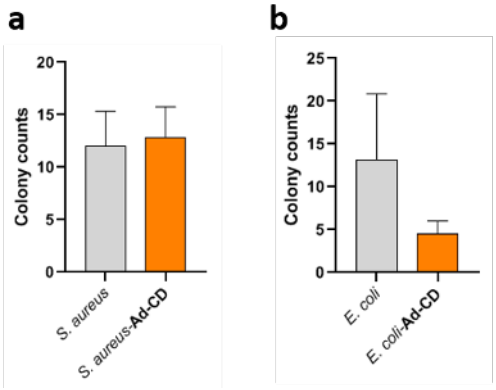

Figure 5: Effect of $Cy3_{1.5}CD_{100}PIBMA_{389}$ loading on viability of *S. aureus* (a) and *E. coli* (b). After **$Cy3_{1.5}CD_{100}PIBMA_{389}$** loading of bacteria ten-fold serial dilutions were prepared and plated in 10 µL aliquots onto BHI agar plates. These plates were incubated overnight, whereafter colonies at the appropriate dilution were counted. Counts are shown as the mean ± standard deviation of loaded (orange) versus unloaded (grey) bacteria in a representative experiment of n = 6. Ad = adamantane; CD = **$Cy3_{1.5}CD_{100}PIBMA_{389}$**.

$Cy3_{1.5}CD_{100}PIBMA_{389}$ loading does not interfere with the core functionalities of monocyte-derived macrophages

To assess whether **$Cy3_{1.5}CD_{100}PIBMA_{389}$** loading adversely affects the functioning of (sentinel) immune cells, we first examined via confocal microscopy the response of monocyte-derived macrophages (MoMΦ) to our **$Cy3_{1.5}CD_{100}PIBMA_{389}$**-loaded MAA/bacteria. **$Cy3_{1.5}CD_{100}PIBMA_{389}$**-loaded MAA particles were readily phagocytosed within 10 minutes, an illustration of which can be seen in Figure 6a. Quantitated phagocytosis of **$Cy3_{1.5}CD_{100}PIBMA_{389}$**-loaded MAA vs control particles showed the two phagocytosed in comparable quantities (37.5±13.6% vs 30.1±9.9%, p = 0.491). Similarly, we found that **$Cy3_{1.5}CD_{100}PIBMA_{389}$**-loaded *S. aureus* (Figure 6b) and *E. coli* (Figure 6c) were phagocytosed within 10 minutes, quantitation of which again showed comparable uptake between loaded and control *S. aureus* (11.1±2.4 vs 14.3±2.7 A.U., p = 0.194) and *E. coli* (7.1±1.6 vs 9.6±3.2 A.U., p = 0.284).

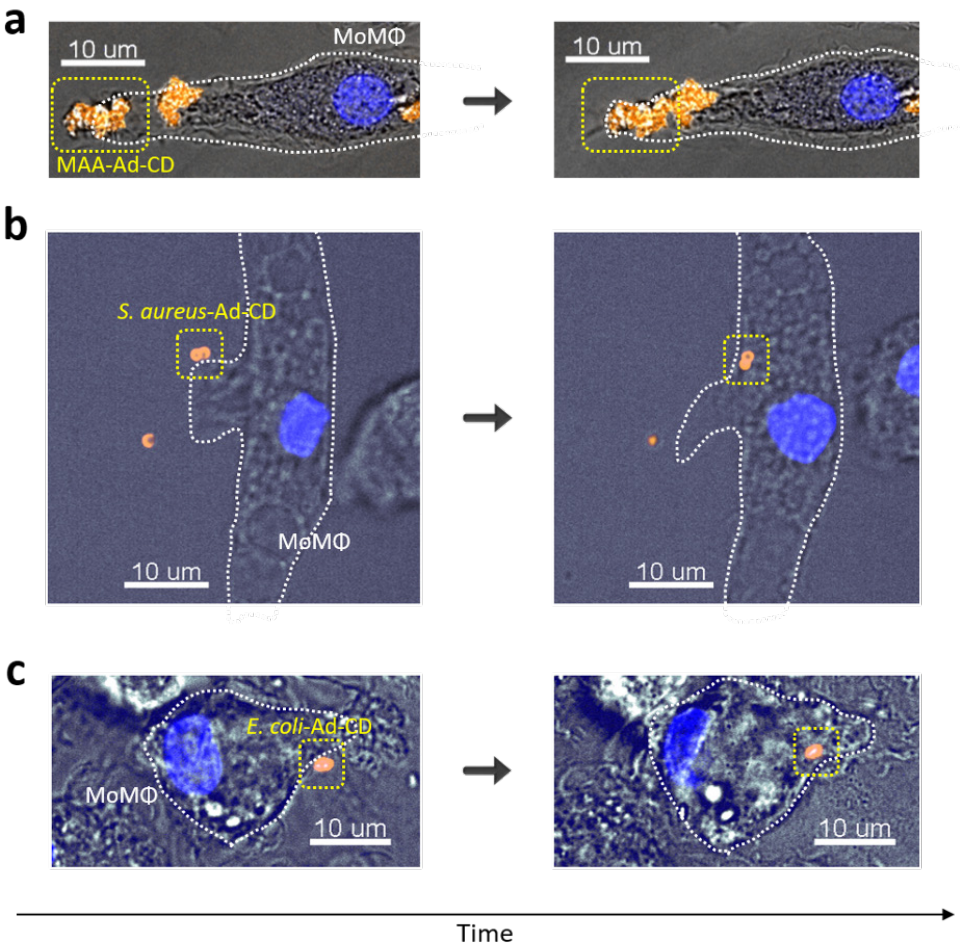

Figure 6: Phagocytic response of MoMΦ to $Cy3_{1.5}CD_{100}PIBMA_{389}$-loaded MAA (a), *S. aureus* (b) and *E. coli* (c). Snapshots demonstrating phagocytic uptake by MoMΦ over a course of about 10 minutes. Ad = adamantane; CD = **$Cy3_{1.5}CD_{100}PIBMA_{389}$**; MAA = macro-aggregated albumin; MoMΦ = monocyte-derived macrophage.

We next assayed the effects of loaded **$Cy3_{1.5}CD_{100}PIBMA_{389}$** on the typical effector functions of MoMΦ: surface marker expression and cytokine production. When stimulated with **$Cy3_{1.5}CD_{100}PIBMA_{389}$**-loaded MAA particles, MoMΦ displayed similar dose-dependent responses in surface marker expression of

CD25 and PDL-1 as seen in response to control MAA particles. At high particle concentrations (1:1 ratio with MoMΦ) both CD25 (2.20±0.55 vs 1.25±0.22 fold-change, Figure 7ai) and PDL-1 (3.02±0.35 vs 1.90±0.19 fold-change, Figure 7aii) expression were elevated in response to **$Cy3_{1.5}CD_{100}PIBMA_{389}$**-loaded MAA particles. Cytokine production also showed increases in TNF-α (281.1±197.8 vs 87.8±48.4 pg/mL, Figure 8ai) and IL-6 (1,402±269.3 vs 616.7±135.6 pg/mL, Figure 8aii) in response to **$Cy3_{1.5}CD_{100}PIBMA_{389}$**-loaded MAA particles at a 1:1 ratio with MoMΦ. However, both increases in surface marker expression and cytokine production were not comparable to responses in positive controls (LPS and IFN-γ stimulated MoMΦ), suggesting that their relevance might be limited. Analogous results were obtained when MoMΦ were stimulated with soluble **$Cy3_{1.5}CD_{100}PIBMA_{389}$** alone (data not shown).

Similar responses were seen in MoMΦ exposed to **$Cy3_{1.5}CD_{100}PIBMA_{389}$**-loaded versus control *S. aureus*. Dose-dependent increases in surface marker expression were again elevated in response to **$Cy3_{1.5}CD_{100}PIBMA_{389}$**-loaded *S. aureus*, especially at high concentrations (4:1 ratio of bacteria to MoMΦ), as seen with increases for CD25 (2.27±0.56 vs 1.4±0.29 fold-change, Figure 7bi) and PDL-1 (2.58±0.49 vs 1.46±0.28 fold-change, Figure 7bii) expression. Cytokine production showed a similar dose-dependent pattern, which at a 4:1 ratio of bacteria to MoMΦ resulted in increases in TNF-α (518.67±394.8 vs 216.7±81.1 pg/mL, Figure 8bi) and IL-6 (28.1±23.9 vs 4.1±4.9 ng/mL, Figure 8bii). Notably, cytokine production was also influenced by Ad functionalization itself: TNF-α production in response to Ad-functionalized *S. aureus* was nearly as high at a 4:1 ratio as that seen in response to **$Cy3_{1.5}CD_{100}PIBMA_{389}$**-loaded *S. aureus* (319.6±197.6 vs 518.67±394.8 pg/mL, Figure 8bi), and IL-6 production was comparable (29.1±19.5 vs 28.1±23.9 ng/mL, Figure 8bii). At lower (1:1 ratio) bacterial concentrations, TNF-α production was actually somewhat higher in response to Ad-functionalized *S. aureus* versus **$Cy3_{1.5}CD_{100}PIBMA_{389}$**-loaded *S. aureus* (447.2±511.9 vs 276.0±326.3 pg/mL, Figure 8bi). As with MAA, these increases were of minor magnitudes compared to increases seen in LPS and IFN-γ stimulated positive controls.

Responses to **$Cy3_{1.5}CD_{100}PIBMA_{389}$**-loaded *E. coli* mostly paralleled the dose-dependent responses seen with MAA and *S. aureus*. Dose-dependent increases elevated over control *E. coli* were observed for both CD25 and PDL-1 expression. These increases were however relatively small compared to the already robust responses to control bacteria (as is typical of *E. coli*), as seen at high bacterial concentrations (4:1 ratio of bacteria to MoMΦ) for both CD25 (8.02±1.51 vs 6.84±0.79 fold-change, Figure 7ci) and PDL-1 (5.97±1.06 vs 4.69±0.81 fold-change, Figure 7cii). Cytokine production with respect to TNF-α was unaffected by loaded **$Cy3_{1.5}CD_{100}PIBMA_{389}$** even at high bacterial concentrations of 4:1 (2,043±942 vs 2,898±919 pg/mL, Figure 8ci). IL-6 production was also com-

parable between **Cy3$_{1.5}$CD$_{100}$PIBMA$_{389}$**-loaded and control *E. coli* at high bacterial concentrations (4:1); however, at lower bacterial concentrations (1:1 ratio) loaded **Cy3$_{1.5}$CD$_{100}$PIBMA$_{389}$** and Ad functionalization appeared to depress IL-6 production (7.6±6.1 vs 22.5±16.5 ng/mL, Figure 8cii).

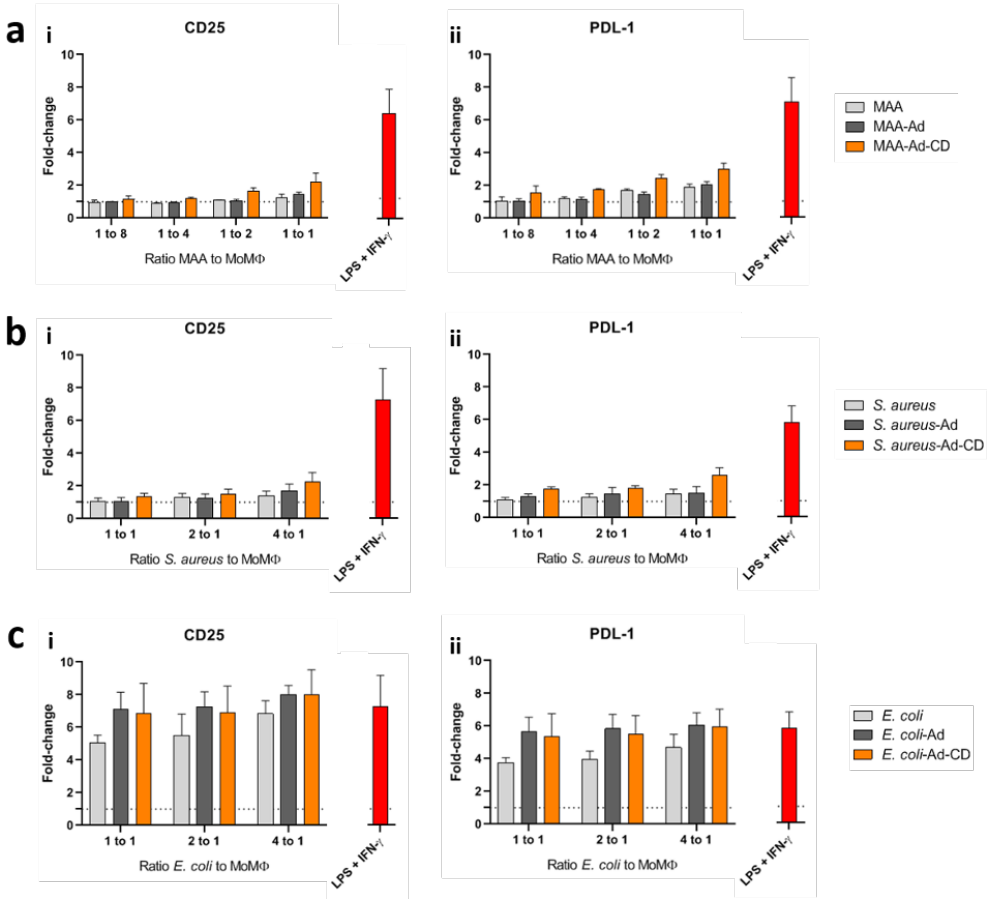

Figure 7: Surface marker responses of MoMΦ to Cy3$_{1.5}$CD$_{100}$PIBMA$_{389}$-loaded MAA (a), *S. aureus* (b) or *E. coli* (c). Expression levels of CD25 **(i)** and PDL-1 **(ii)** given as fold-change of median fluorescent intensity versus baseline expression in unstimulated MoMΦ by flow cytometry. Control MAA/bacteria are given in light grey, Ad-functionalized controls in dark grey, and loaded MAA/bacteria in orange; positive controls stimulated with LPS and IFN-γ are shown in red. Data are represented as means ± standard deviation for representative experiments of n = 3. MAA = macro-aggregated albumin; MoMΦ = monocyte-derived macrophages; Ad = adamantane.

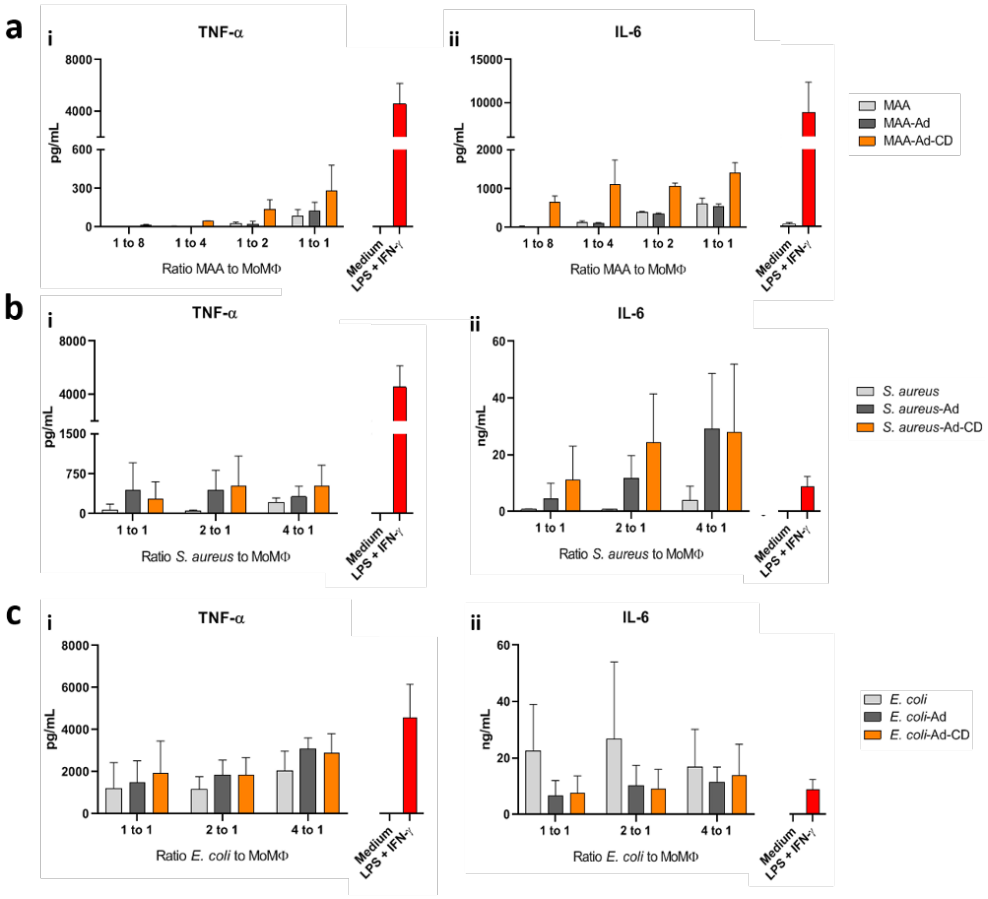

Figure 8: Cytokine responses of MoMΦ to $Cy3_{1.5}CD_{100}PIBMA_{389}$-loaded MAA (a), *S. aureus* (b) or *E. coli* (c). Concentrations of the cytokines TNF-α **(i)** and IL-6 **(ii)** in MoMΦ culture supernatants 24 hours after stimulation, as measured via ELISA. Control MAA/bacteria are given in light grey, Ad-functionalized controls in dark grey, and loaded MAA/bacteria in orange. MoMΦ stimulated with medium (beige) or LPS and IFN-γ (red) served as negative and positive controls, respectively. Data shown are means ± standard deviation for representative experiments of n = 3. MAA = macro-aggregated albumin; MoMΦ = monocyte-derived macrophages; Ad = adamantane.

Discussion

The present study shows that supramolecular host-guest chemistry can be effectively harnessed to load both Gram-positive and-negative bacterial surfaces with a versatile chemical scaffold. The scaffold **$Cy3_{1.5}CD_{100}PIBMA_{389}$** loaded

onto bacteria did not impair immune recognition of these bacteria by MoMΦs, as gauged by phagocytic capacity, surface marker expression and cytokine production. This technology may thus be an attractive platform for future investigations requiring precise introduction of immunomodulatory components onto bacterial pathogens.

Existing strategies for modifying bacterial surfaces have generally relied on covalently binding moieties of interest to either cell surface amines/thiols or unnatural chemical ligands, such as aldehydes, introduced metabolically (Bi et al., 2018; Dumont et al., 2012; Taherkhani et al., 2014). Our modification method demonstrates that non-covalent chemistry harnessing supramolecular interactions between CD and Ad is equally able to modify bacterial surfaces, and unlike covalent binding does not generally perturb normal functioning of e.g. cell surface proteins (Bi et al., 2018). Introduction of Ad functionalization on the surface of MAA and bacteria significantly promoted the loading of **$Cy3_{1.5}CD_{100}PIBMA_{389}$**, particularly for the Gram-positive *S. aureus*, probably because these bacteria lack the highly heterogenous constituents of Gram-negative surfaces containing certain hydrophobic structures able to mimic Ad's supramolecular interactions with CD (Hooda and Moraes, 2018; Rood et al., 2017; Thanassi et al., 2012; Whitfield and Trent, 2014).

We found that our cell surface modification method preserved the capacity of MoMΦs to engage and recognize **$Cy3_{1.5}CD_{100}PIBMA_{389}$**-loaded MAA and bacteria. Phagocytosis of **$Cy3_{1.5}CD_{100}PIBMA_{389}$**-loaded MAA and bacteria was not inhibited by the presence of CD carbohydrates, an important finding for possible future application of the technology to introduce immunomodulatory components onto bacteria. MoMΦs that phagocytosed **$Cy3_{1.5}CD_{100}PIBMA_{389}$**-loaded MAA and bacteria retained their ability to respond normally to these entities as gauged by surface marker expression and cytokine production. This was most evident in analyzing responses to *E. coli*: robust CD25 and PDL-1 expression and TNF-α production were seen for both control and **$Cy3_{1.5}CD_{100}PIBMA_{389}$**-loaded *E. coli*. Altogether, these findings suggest our **$Cy3_{1.5}CD_{100}PIBMA_{389}$** chemical scaffolds are well-suited for introducing modifications onto bacterial surfaces and can be used to investigate interactions between bacteria and the immune system.

An unexpected finding to emerge from this study was that our **$Cy3_{1.5}CD_{100}PIBMA_{389}$** scaffolds are in themselves somewhat immunogenic. We generally observed dose-dependently increased pro-inflammatory responses to **$Cy3_{1.5}CD_{100}PIBMA_{389}$**-loaded MAA, *S. aureus* and *E. coli*. Remarkably, these increases were most evident with MAA. However, the increases were also notable in bacteria, especially *S. aureus*, with respect to cytokine production. Such disparities between surface markers and cytokines are reflective of the complexity of assess-

ing immune processes using simplified *in vitro* models and indicate the need to ultimately fully evaluate immune responses in more representative *in vivo* models. The immunogenicity of **Cy3**$_{1.5}$**CD**$_{100}$**PIBMA**$_{389}$ is likely mediated by its CD carbohydrates, as studies have identified various immunogenic carbohydrate structures in plants, bacteria and parasites (Matsuo et al., 2014; Pazur and Forsberg, 1980; Weiss et al., 1986). This is a natural consequence of the important role that carbohydrate diversity plays in recognition of self and non-self structures (Amon et al., 2014; Moremen et al., 2012). In addition, Ad$_2$-UBI$_{29-41}$ alone also seemed to have a mildly proinflammatory potential as suggested by the cytokine profiles, possibly mediated by the hydrocarbon components (Brinchmann et al., 2018; Michael et al., 2013; Osgood et al., 2017). While these unexpected immunogenic properties were interesting to note, they were very modest compared to positive controls and as such are unlikely to significantly impact implementation of the presented technology.

Theoretically, the presented technology could be utilized as a tool for adjuvanting (bacterial) whole-organism vaccines. Although whole-organism vaccines generally have less attractive safety profiles, they may be considered for diseases where subunit vaccines provide insufficient protection. The presented technology provides a means of further boosting immune responses to intact bacterial vaccines by physically conjugating immunogenic adjuvants. For instance, introducing LPS-like immunogens onto whole-organism vaccines could, analogously to subunit vaccinology, enhance the immunogenicity of any bacterium.

In conclusion, we have here shown that supramolecular host-guest chemistry between CD and Ad can be utilized to efficiently load versatile chemical scaffolds onto both Gram-positive and negative bacteria, and that these scaffolds are well-tolerated by a canonical immune cell. We thus believe this method provides a useful tool for future investigations seeking to alter the immunogenic properties of (bacterial) pathogens for the purposes of either dissecting the complex host-pathogen interactions involved in infectious disease etiology or developing novel interventions against infectious diseases.

References

Amon, R., Reuven, E.M., Leviatan Ben-Arye, S., and Padler-Karavani, V. (2014). Glycans in immune recognition and response. Carbohydr Res *389*, 115-122.

Annane, D., Bellissant, E., and Cavaillon, J.M. (2005). Septic shock. Lancet *365*, 63-78.

Bekeredjian-Ding, I., Stein, C., and Uebele, J. (2017). The Innate Immune Response Against Staphylococcus aureus. Curr Top Microbiol Immunol *409*, 385-418.

Bi, X., Yin, J., Chen Guanbang, A., and Liu, C.F. (2018). Chemical and Enzymatic Strategies for Bacterial and Mammalian Cell Surface Engineering. Chemistry *24*, 8042-8050.

Brinchmann, B.C., Skuland, T., Rambol, M.H., Szoke, K., Brinchmann, J.E., Gutleb, A.C., Moschini, E., Kubatova, A., Kukowski, K., Le Ferrec, E.*, et al.* (2018). Lipophilic components of diesel exhaust particles induce pro-inflammatory responses in human endothelial cells through AhR dependent pathway(s). Part Fibre Toxicol *15*, 21.

Dumont, A., Malleron, A., Awwad, M., Dukan, S., and Vauzeilles, B. (2012). Click-mediated labeling of bacterial membranes through metabolic modification of the lipopolysaccharide inner core. Angew Chem Int Ed Engl *51*, 3143-3146.

Faria, M., Bjornmalm, M., Thurecht, K.J., Kent, S.J., Parton, R.G., Kavallaris, M., Johnston, A.P.R., Gooding, J.J., Corrie, S.R., Boyd, B.J.*, et al.* (2018). Minimum information reporting in bio-nano experimental literature. Nat Nanotechnol *13*, 777-785.

Gautam, S., Gniadek, T.J., Kim, T., and Spiegel, D.A. (2013). Exterior design: strategies for redecorating the bacterial surface with small molecules. Trends Biotechnol *31*, 258-267.

Goldmann, O., and Medina, E. (2018). Staphylococcus aureus strategies to evade the host acquired immune response. Int J Med Microbiol *308*, 625-630.

Gonzalez-Campo, A., Hsu, S.H., Puig, L., Huskens, J., Reinhoudt, D.N., and Velders, A.H. (2010). Orthogonal covalent and noncovalent functionalization of cyclodextrin-alkyne patterned surfaces. J Am Chem Soc *132*, 11434-11436.

Hooda, Y., and Moraes, T.F. (2018). Translocation of lipoproteins to the surface of gram negative bacteria. Curr Opin Struct Biol *51*, 73-79.

Kong, N.C., Beran, J., Kee, S.A., Miguel, J.L., Sanchez, C., Bayas, J.M., Vilella, A., Calbo-Torrecillas, F., Lopez de Novales, E., Srinivasa, K.*, et al.* (2008). A new adjuvant improves the immune response to hepatitis B vaccine in hemodialysis patients. Kidney Int *73*, 856-862.

Kumar, H., Kawai, T., and Akira, S. (2011). Pathogen recognition by the innate immune system. Int Rev Immunol *30*, 16-34.

Maldonado, R.F., Sa-Correia, I., and Valvano, M.A. (2016). Lipopolysaccharide modification in Gram-negative bacteria during chronic infection. FEMS Microbiol Rev *40*, 480-493.

Matsuo, K., Kagaya, U., Itchoda, N., Tabayashi, N., and Matsumura, T. (2014). Deletion of plant-specific sugar residues in plant N-glycans by repression of GDP-D-mannose 4,6-dehydratase and beta-1,2-xylosyltransferase genes. J Biosci Bioeng *118*, 448-454.

Michael, S., Montag, M., and Dott, W. (2013). Pro-inflammatory effects and oxidative stress in lung macrophages and epithelial cells induced by ambient particulate matter. Environ Pollut *183*, 19-29.

Mogensen, T.H. (2009). Pathogen recognition and inflammatory signaling in innate immune defenses. Clin Microbiol Rev *22*, 240-273, Table of Contents.

Mongis, A., Piller, F., and Piller, V. (2017). Coupling of Immunostimulants to Live Cells through Metabolic Glycoengineering and Bioorthogonal Click Chemistry. Bioconjug Chem *28*, 1151-1165.

Moremen, K.W., Tiemeyer, M., and Nairn, A.V. (2012). Vertebrate protein glycosylation: diversity, synthesis and function. Nat Rev Mol Cell Biol *13*, 448-462.

Naber, C.K. (2009). Staphylococcus aureus bacteremia: epidemiology, pathophysiology, and management strategies. Clin Infect Dis *48 Suppl 4*, S231-237.

Neirynck, P., Brinkmann, J., An, Q., van der Schaft, D.W., Milroy, L.G., Jonkheijm, P., and Brunsveld, L. (2013). Supramolecular control of cell adhesion via ferrocene-cucurbit[7]uril host-guest binding on gold surfaces. Chem Commun (Camb) *49*, 3679-3681.

Osgood, R.S., Upham, B.L., Bushel, P.R., Velmurugan, K., Xiong, K.N., and Bauer, A.K. (2017). Secondhand Smoke-Prevalent Polycyclic Aromatic Hydrocarbon Binary Mixture-Induced Specific Mitogenic and Pro-inflammatory Cell Signaling Events in Lung Epithelial Cells. Toxicol Sci *157*, 156-171.

Paavonen, J., Naud, P., Salmeron, J., Wheeler, C.M., Chow, S.N., Apter, D., Kitchener, H., Castellsague, X., Teixeira, J.C., Skinner, S.R.*, et al.* (2009). Efficacy of human papillomavirus (HPV)-16/18 AS04-adjuvanted vaccine against cervical infection and precancer caused by oncogenic HPV types (PATRICIA): final analysis of a double-blind, randomised study in young women. Lancet *374*, 301-314.

Pazur, J.H., and Forsberg, L.S. (1980). The sugar sequence of a streptococcal, immunogenic tetraheteroglycan: a revision. Carbohydr Res *83*, 406-408.

Rodell, C.B., Mealy, J.E., and Burdick, J.A. (2015). Supramolecular Guest-Host Interactions for the Preparation of Biomedical Materials. Bioconjug Chem *26*, 2279-2289.

Rood, M.T., Spa, S.J., Welling, M.M., Ten Hove, J.B., van Willigen, D.M., Buckle, T., Velders, A.H., and van Leeuwen, F.W. (2017). Obtaining control of cell surface functionalizations via Pre-targeting and Supramolecular host guest interactions. Sci Rep *7*, 39908.

Spa, S.J., Welling, M.M., van Oosterom, M.N., Rietbergen, D.D.D., Burgmans, M.C., Verboom, W., Huskens, J., Buckle, T., and van Leeuwen, F.W.B. (2018). A Supramolecular Approach for Liver Radioembolization. Theranostics *8*, 2377-2386.

Taherkhani, S., Mohammadi, M., Daoud, J., Martel, S., and Tabrizian, M. (2014). Covalent binding of nanoliposomes to the surface of magnetotactic bacteria for the synthesis of self-propelled therapeutic agents. ACS Nano *8*, 5049-5060.

Thanassi, D.G., Bliska, J.B., and Christie, P.J. (2012). Surface organelles assem-

bled by secretion systems of Gram-negative bacteria: diversity in structure and function. FEMS Microbiol Rev *36*, 1046-1082.

Weiss, J.B., Magnani, J.L., and Strand, M. (1986). Identification of Schistosoma mansoni glycolipids that share immunogenic carbohydrate epitopes with glycoproteins. J Immunol *136*, 4275-4282.

Welling, M.M., Spa, S.J., van Willigen, D.M., Rietbergen, D.D.D., Roestenberg, M., Buckle, T., and van Leeuwen, F.W.B. (2019). In vivo stability of supramolecular host-guest complexes monitored by dual-isotope multiplexing in a pre-targeting model of experimental liver radioembolization. J Control Release *293*, 126-134.

Welling, M.M., Visentin, R., Feitsma, H.I., Lupetti, A., Pauwels, E.K., and Nibbering, P.H. (2004). Infection detection in mice using 99mTc-labeled HYNIC and N2S2 chelate conjugated to the antimicrobial peptide UBI 29-41. Nucl Med Biol *31*, 503-509.

Whitfield, C., and Trent, M.S. (2014). Biosynthesis and export of bacterial lipopolysaccharides. Annu Rev Biochem *83*, 99-128.

Willyard, C. (2017). The drug-resistant bacteria that pose the greatest health threats. Nature *543*, 15.

Wolf, A.J., and Underhill, D.M. (2018). Peptidoglycan recognition by the innate immune system. Nat Rev Immunol *18*, 243-254.

Wynn, T.A., Chawla, A., and Pollard, J.W. (2013). Macrophage biology in development, homeostasis and disease. Nature *496*, 445-455.

Methods

Preparation of $Cy3_{1.5}CD_{100}PIBMA_{389}$-bound protein aggregates and bacteria

The material characteristics of **$Cy3_{1.5}CD_{100}PIBMA_{389}$** in the context of these experiments as per recommended guidelines (Faria et al., 2018) are as follows. **$Cy3_{1.5}CD_{100}PIBMA_{389}$** synthesis was accomplished by grafting the nucleophiles β-CD-NH_2 and Cy3-NH_2 onto the anhydrides of poly(isobutylene-*alt*-maleic-anhydride) in a solution of dry DMSO together with DIPEA, followed by hydrolyzing the non-reacted anhydrides to carboxylates. Thereafter, ethanolamine was conjugated to the free carboxylates via an amide linkage backbone in order to sequester the carboxylates' negative charges, and the product purified by dialysis. The exact conditions used can be found as previously described (Rood et al., 2017). ^{1}H-NMR and NMR Diffusion Ordered Spectroscopy (DOSY) determined the product to contain about 100 β-CD units and 1.5 Cy3 units. The product, in linear form, was estimated to be about 240 nm long and 4 nm wide, with a weight of approximately 190 kDa.

To first bind **$Cy3_{1.5}CD_{100}PIBMA_{389}$** to macro-aggregated albumin (MAA), a protein aggregate representing a simplified bacterium, 100 µL MAA (2 mg/mL) (TechneScan LyoMAA, London, UK) was sonicated (to break up larger aggregates), added to 100 µL of a 1 µM solution of Ad-TFP (tri(2-furyl)phosphine) in PBS supplemented with 2 mg/mL bovine serum albumin (BSA) and incubated for 30 minutes at 37 °C with shaking. The reaction mixture was centrifuged at 1,600 RCF for 3 minutes, supernatant removed and the pellet resuspended in 1 mL PBS with BSA; washing was repeated twice. Subsequently, the pellet was resuspended in 100 µL of a 1 µM solution of **$Cy3_{1.5}CD_{100}PIBMA_{389}$** in PBS and incubated for 60 minutes at 37 °C with shaking. Subsequently, this mixture was similarly washed three times by centrifuging at 1,600 RCF for 3 minutes, removing supernatant and resuspending the pellet in 1 mL PBS with BSA. After resuspending the product in 100 µL PBS with BSA, the concentration in units of particles/mL was determined using a Bürker counting chamber. This value was used to prepare eventual dilutions in RPMI (Life Sciences™ GIBCO®, Thermo Fischer Scientific, Waltham, MA, USA) + 10% fetal bovine serum (FBS) (Capricorn Scientific, Ebsdorfergrund, Germany) for analysis by confocal microscopy and flow cytometry.

To initially bind **$Cy3_{1.5}CD_{100}PIBMA_{389}$** to bacteria using Ad functionalization introduced via cell surface lysine residues, 10^7 bacteria (*Staphylococcus aureus* and *Escherichia coli*) were added to 100 µL of a 1 µM solution of Ad-TFP in PBS (also containing 10 µM Hoechst 33342 (Sigma-Aldrich (St. Louis, MO, USA)) and incubated for 30 minutes at 37 °C with shaking. The reaction mixture was then

centrifuged at 10,000 RCF for 5 minutes, supernatant was removed, and the pellet resuspended in 1 mL PBS; washing was repeated twice. After washing, the pellet was resuspended in 100 μL of a 1 μM solution of **$Cy3_{1.5}CD_{100}PIBMA_{389}$** in PBS and incubated for 60 minutes at 37 °C with shaking. The mixture was then washed thrice with PBS as described above. After washing, the pellet was resuspended in 100 μL PBS and analyzed by confocal microscopy.

To alternatively bind **$Cy3_{1.5}CD_{100}PIBMA_{389}$** to bacteria using Ad functionalization introduced via a membrane-adhering ubiquicidin peptide (UBI_{29-41}), 10^7 bacteria were added to 100 μL of a 8 μM solution of UBI-Ad_2 in 25 mM ammonium acetate buffer pH 5 (also containing 10 μM Hoechst 33342) and incubated for 30 minutes at 37 °C with shaking. The mixture was then centrifuged at 10,000 RCF for 5 minutes, supernatant was removed, and the pellet resuspended in PBS; washing was repeated twice. Subsequently, the pellet was resuspended in 100 μL of a 1 μM solution of **$Cy3_{1.5}CD_{100}PIBMA_{389}$** in PBS and incubated for 30 minutes at 37 °C with shaking. The mixture was then washed 3 times in PBS, and finally resuspended in 100 μL RPMI + 10% FBS to create a stock solution used to prepare dilutions in RPMI + 10% FBS for analysis by confocal microscopy and flow cytometry.

Analysis of $Cy3_{1.5}CD_{100}PIBMA_{389}$-bound protein aggregates and bacteria

$Cy3_{1.5}CD_{100}PIBMA_{389}$ bound to MAA or bacteria was first qualitatively detected by confocal microscopy performed on a Leica Sp8 WLL confocal microscope using LAS X software. Prior to microscopy, 10 μL inoculums containing ~10^6 units MAA or bacteria were added to glass bottom microwell dishes (MatTek Corporation, Ashland, MA, USA), overlaid with 1% agarose pads (to eliminate Brownian motion interfering with digital image acquisition), and finally overlaid with a coverslip.

Quantitation of Ad functionalization and **$Cy3_{1.5}CD_{100}PIBMA_{389}$** binding efficiency was performed by flow cytometry on BD (Franklin Lakes, NJ, USA) LSRFortessa ™ X-20 or FACSCanto II instruments using FACSDiva ™ software using the abovementioned procedures and reagents or analogues thereof. Bacteria were isolated from debris by gating on their Hoechst signal.

To assess the viability of **$Cy3_{1.5}CD_{100}PIBMA_{389}$**-bound bacteria, $6.4x10^6$ CFU/mL bacteria underwent the abovementioned procedure. These bacteria were then serially diluted 10-fold and 10 μL inoculums from each dilution pipetted onto BHI agar plates. These plates were cultured overnight at 37 °C, after which colonies on plates were counted.

Analysis of phagocytic responses

MoMΦ were prepared as follows. Peripheral blood from volunteers was diluted 1:1 with room temperature HBSS (Life Sciences™ GIBCO®) containing 100 U/mL penicillin and 100 μg/mL streptomycin. Ficoll (Apotheek AZL, Lokeren, The Netherlands) was added underneath diluted blood and samples were spun at 400 RCF for 25 minutes with slow deceleration. Peripheral blood mononuclear cells (PBMCs) above the Ficoll phase were carefully isolated with a Pasteur pipette and diluted 1:1 with HBSS + 1% fetal bovine serum (FBS). PBMCs were spun at 200 RCF for 20 minutes. Supernatant was removed, and the pellet resuspended in HBSS + 1% FBS. PBMCs were again spun at 200 RCF for 20 minutes. Supernatant was removed, and the pellet resuspended in MACS buffer (PBS + 0.5% BSA + 2 mM EDTA). After PBMCs were counted, PBMCs were centrifuged at 300 RCF at 4 °C for 10 minutes. Supernatant was removed, and cells were resuspended in 95 μL/10^7 cells MACS buffer. To this suspension 5 μL/10^7 cells Miltenyi Biotec MACS CD14 MicroBeads (Cologne, Germany) were added. PBMCs were then incubated for 15 minutes at 4 °C. After incubation, cells were washed with MACS buffer and centrifuged at 300 RCF at 4°C for 10 minutes. Supernatant was removed, cells were resuspended in 1 mL MACS buffer, and the suspension was run through a Miltenyi Biotec MACS LS column attached to a magnetic separator. The column was washed thrice with MACS buffer. After removing the column from the magnetic separator, the column was flushed with RPMI (Life Sciences™ GIBCO®) containing 100 U/mL penicillin and 100 μg/mL streptomycin. Monocytes were centrifuged at 300 RCF at 4 °C for 10 minutes. After removing supernatant, monocytes were resuspended in RPMI + 10% FBS and counted.

To differentiate monocytes into macrophages, monocytes were plated at a density of 400.000 cells/mL in RPMI + 10% FBS supplemented with 20 ng/mL macrophage colony-stimulating factor and incubated at 37 °C. After 2-3 days, medium was refreshed. After 6 days, macrophages were resuspended by scraping with a pipette tip and counted, whereafter they were ready for downstream applications.

Confocal microscopy was performed on a Leica Sp8 WLL confocal microscope using LAS X software. One day prior to microscopy, $5*10^4$ MoMΦ were incubated on glass bottom microwell dishes (MatTek Corporation) in a 200 μL drop of RPMI + 10% FBS for 2 hours at 37 °C. Once MoMΦ had adhered, an additional 1.8 mL RPMI + 10% FBS was added, and MoMΦ were incubated at 37 °C overnight. Immediately prior to microscopy the next day, RPMI + 10% FBS was removed from the confocal dish, a 10 μL inoculum added to the MoMΦ, and a coverslip overlaid on the cells. MoMΦ behavior was then analyzed in a 37 °C environment.

Analysis of immune responses

All experiments were performed in triplicate. MoMΦ post-harvesting were plated at a density of 10^5 cells/100 µL in 96-well plates (Thermo Fischer Scientific) and incubated for 24 hours at 37 °C. Thereafter, MoMΦ were stimulated with 100 µL of various MAA/*S. aureus*/*E. coli*-Ad-CD dilutions and allowed to incubate another 24 hours at 37 °C. Subsequently, supernatants were removed and stored for eventual cytokine analysis. Wells were filled with cold PBS, and cells harvested by scraping with a pipette tip and transferring to a FACS V-bottom plate (Thermo Fischer Scientific). Cells were centrifuged at 350 RCF and 4 °C for 4 minutes and supernatant discarded. Pellets were resuspended in 50 µL Aqua solution (Thermo Fisher Scientific) and incubated on ice for 20 minutes. Thereafter, 150 µL 1.9% paraformaldehyde was added, and cells incubated on ice for 15 minutes. Cells were centrifuged at 350 RCF and 4 °C for 4 minutes and supernatant discarded. Pellets were resuspended in 200 µL PBS, centrifuged at 350 RCF and 4 °C for 4 minutes, and supernatant discarded. Pellets were then resuspended in 30 µL antibody mix and incubated for 30 minutes at 4 °C. After incubation, 170 µL PBS was added, cells were centrifuged at 350 RCF and 4 °C for 4 minutes, and supernatant was discarded. Pellets were resuspended in 50 µL FACS buffer (PBS + 0.5% BSA + 2 mM EDTA) and transferred to 1.4 mL FACS tubes. These samples were then run through a BD LSRFortessa ™ X-20 using BD FACSDiva ™ software.

Cytokine production in MoMΦ culture supernatants was assayed using kits from BD Biosciences; specifically, Human TNF ELISA Set (Cat. No. 555212) and Human IL-6 ELISA Set (Cat. No. 555220) kits were used according to the manufacturer's specifications and analyzed by a Thermo Fischer Scientific Multiskan FC plate reader.

Statistical analysis

Mean values were compared by Student's t-test performed using SPSS 25 software (IBM, Armonk, NY, USA).

Acknowledgments

The authors would like to acknowledge Sven van Leeuwen for helping generate the superlative graphics used in this paper.

Funding

The research leading to these results has received funding from a ZONMW VENI grant (016.156.076) financed by the Netherlands Organization for Scientific Research (NWO) and an LUMC PhD project grant (18-1919).